JACS
JOURNAL OF THE AMERICAN CHEMICAL SOCIETY
Article
pubs.acs.org/JACS

Influence of the Selectivity Filter Properties on Proton Selectivity in the Influenza A M2 Channel

Todor Dudev,*[,†,§] Cédric Grauffel,[†] and Carmay Lim*[,†,‡]

[§]Faculty of Chemistry and Pharmacy, Sofia University, Sofia 1164, Bulgaria
[†]Institute of Biomedical Sciences, Academia Sinica, Taipei 11529, Taiwan
[‡]Department of Chemistry, National Tsing Hua University, Hsinchu 300, Taiwan

Supporting Information

ABSTRACT: The homotetrameric M2 proton channel of influenza A plays a crucial role in the viral life cycle and is thus an important therapeutic target. It selectively conducts protons against a background of other competing cations whose concentrations are up to a million times greater than the proton concentration. Its selectivity is largely determined by a constricted region of its open pore known as the selectivity filter, which is lined by four absolutely conserved histidines. While the mechanism of proton transport through the channel has been studied, the physical principles underlying the selectivity for protons over other cations in the channel's His_4 selectivity filter remain elusive. Furthermore, it is not known if proton selectivity absolutely requires all four histidines with two of the four histidines protonated and if other titratable amino acid residues in lieu of the histidines could bind protons and how they affect proton selectivity. Here, we elucidate how the competition between protons and rival cations such as Na^+ depends on the selectivity filter's (1) histidine protonation state, (2) solvent exposure, (3) oligomeric state (the number of protein chains and thus the number of His ligands), and (4) ligand composition by evaluating the free energies for replacing monovalent Na^+ with H_3O^+ in various model selectivity filters. We show that tetrameric His_4 filters are more proton-selective than their trimeric His_3 counterparts, and a dicationic His_4 filter where two of the four histidines are protonated is more proton-selective than tetrameric filters with other charge states/composition (different combinations of His protonation states or different metal-ligating ligands). The $[His_4]^{2+}$ filter achieves proton selectivity by providing suboptimal binding conditions for rival cations such as Na^+, which prefers a neutral or negatively charged filter instead of a dicationic one, and three rather than four ligands with oxygen-ligating atoms.

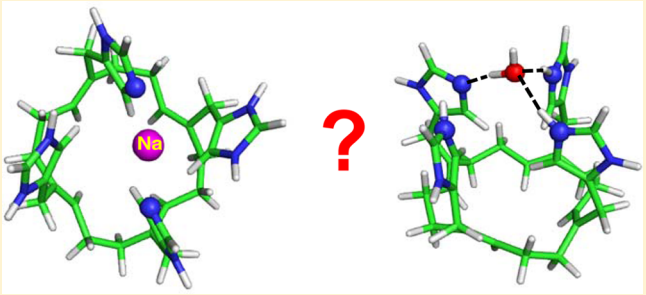

INTRODUCTION

The acid-activated M2 proton channel of influenza A virus (abbreviated as M2A) transports protons across the viral envelope to acidify the virion interior during endocytosis. This step is crucial in the virus life cycle and infection mechanism, as it enables the uncoating of the viral RNA and subsequent viral replication.[1] Thus, the M2A channel is an important pharmaceutical target for antiviral drugs, which, by making the pore defunct, prevent the virus from proliferating. Therefore, an in-depth understanding of its proton transport and selectivity mechanisms would aid in designing/engineering new anti-influenza agents. Unraveling the conductivity and selectivity mechanisms of the M2A channel would also shed light on the basic principles used to evolve protein devices with highly specialized properties.

The M2A channel is an integral membrane protein comprising four monomers that form a proton-conductive pore.[2] Each monomer consists of 97 amino acid (aa) residues with the first 24 and last 37 residues comprising the extracellular N-terminal and intracellular C-terminal domains, while residues 25−43 and 44−60 form the pore-containing transmembrane domain and cytoplasmic amphiphilic helix.[3,4] This architecture with a single-pass transmembrane helix is quite different from the six transmembrane-helix monomeric construct of the voltage-gated ion channels in higher organisms. To fulfill its role as a proton-carrier, the channel should be very selective for the namesake ion, as the proton concentration in the cellular/extracellular milieu is about a million times less than the concentration of other competing ions such as Na^+ or K^+.[5] Indeed, the M2A channel has very high affinity for protons, selecting H^+ over Na^+ or K^+ by $\sim 10^6$.[6−12] Unlike its voltage-gated counterpart in higher organisms, H_v1, which has perfect proton selectivity conducting no other ions except protons,[5] the M2A channel allows for some small Na^+ or K^+ currents.[10−12]

The selectivity of an ion channel is determined mainly by its selectivity filter (SF) − a single or multilayered ring-like structure located at a constricted region of an open pore, comprising conserved aa residues that interact with the passing ion. In the M2A channel, the SF consists of four histidines

Received: August 3, 2016
Published: September 12, 2016

DOI: 10.1021/jacs.6b08041
J. Am. Chem. Soc. 2016, 138, 13038−13047

(His-37) from each of the four α helices.[13−15] His-37 and a nearby Trp-41 implicated in channel gating[16] are absolutely conserved among different sequences of M2A proteins.[17] Mutation of His-37 to other aa residues such as Gly, Ala, Ser, Thr, or Glu resulted in a nonselective channel,[13,15] implying that the [His_4] SF is crucial for proton selectivity. This is also supported by the fact that the proton-selective homotetrameric M2 channel of influenza B virus shares little (18.5%) sequence identity with the M2A channel except for the HXXXW motif. Since the two viral proton channels achieve high proton selectivity despite differences in the overall composition/structure, the [His_4] SF appears to dictate proton selectivity.[18] Such a SF with four histidines is unique in composition among the family of cation-specific ion channels.

As the four conserved histidines in the M2A SF are crucial for proton selectivity, their pK_a values have been established by various research groups using NMR spectroscopy yielding five sets of pK_a values: (i) 8.2 ± 0.2, 8.2 ± 0.2, 6.3 ± 0.3, <5.0[19] and (ii) 7.6 ± 0.1, 6.8 ± 0.1, 4.9 ± 0.3, 4.2 ± 0.6[20] for the M2A transmembrane domain (residues 22−46), (iii) 7.63 ± 0.15, 4.52 ± 0.15[21] for the M2A conductance domain (residues 18−60), (iv) 7.11 ± 0.02, 5.39 ± 0.37[22] for M2A excluding the N-terminal domain (residues 21−97), and (v) 6.3 ± 0.1, 6.3 ± 0.1, and 5.5 ± 0.3[23] for full-length M2A. The variations in the pK_a values reported by different groups reflect the different M2A constructs and membrane compositions. Nevertheless, the pK_a values indicate that at the channel activation pH of ∼6, two of the histidines are likely to be protonated. Protonating a third His residue in the endosome acidic environment triggers proton conduction through the channel.[18,19,24]

Structures of various M2A constructs in different membrane mimetic environments have revealed different geometrical arrangements of the imidazole/imidazolium rings inside the SF.[25] A solid-state NMR structure of M2A (residues 22−62) in a lipid bilayer at pH 7.5 revealed a pair of imidazole-imidazolium rings connected via hydrogen bonds, so-called "dimer-of-dimers" structure (PDB entry 2L0J,[26] Figure 1a). However, a solution NMR structure of rimantadine-bound M2A (residues 18−60) also at pH 7.5 (PDB entry 2RLF[27]) and a 1.65-Å crystal structure of the M2A transmembrane domain (PDB entry 3LBW[28]) at pH 6.5 showed a box-like structure of the SF with no direct hydrogen bonds between imidazole and imidazolium (Figure 1b); instead, the SF structure is stabilized by hydrogen bonds with water molecules above and beneath the plane of the histidine tetrad. More recent NMR experiments support the "His-box" structure with no direct hydrogen bonds between the histidines in the SF.[21,22,24]

Apart from the M2A structure, in particular the protonation states and orientations of the four conserved histidines (His tetrad) in the SF, the mechanism of proton transport through the channel has also been studied, albeit not fully understood. Measurements of the wild-type channel conductance[7,8] and the kinetic isotope effect upon $D_2O \rightarrow H_2O$ replacement[7] have suggested that protons do not pass through the M2A channel as hydronium ions, but interact with titratable groups lining the pore.[18] Two proton transport mechanisms assuming different roles for the titratable histidines lining the SF have been suggested: The "shutter" mechanism postulates that the His tetrad serves as a gate that opens at low pH (due to repulsion among the positively charged imidazolium side chains) and assumes a continuous water wire, allowing the proton to hop from one water molecule to another inside the pore;[29−31] however, this mechanism has not gained much support.[24,32,33]

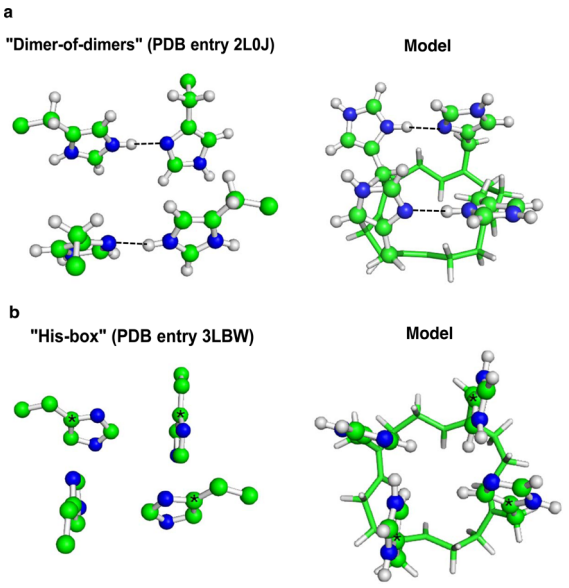

Figure 1. Structures of the $[His_4]^{2+}$ M2A selectivity filter from (a) solid-state NMR (PDB entry 2L0J) and B3-LYP/6-31+G(3d,p) geometry optimization calculations, and (b) X-ray crystallography (PDB entry 3LBW; resolution 1.65 Å) and B3-LYP/6-31+G(3d,p) geometry optimization calculations. The Cγ atom position in each imidazole/imidazolium ring in (b) is marked by an asterisk.

Instead, most studies favor a "His-relay" or "shuttle" mechanism,[34] in which a titratable histidine from the SF transfers a proton from the extracellular region to the intracellular region: First, a deprotonated neutral His-37 accepts a proton from an incoming H_3O^+ (or $H_5O_2^+$ or $H_9O_4^+$), then the same or another protonated His from the SF flips down and donates a proton to a water molecule below the ring of Trp-41 side chains.[20,26,33−43] As the M2A channel is slightly permeable to some monovalent cations such as NH_4^+,[7] Na^+, and K^+,[10−12] another transport mechanism may coexist along with the "His-relay" mechanism for the nonproton species.

In addition to experimental and theoretical studies on the M2A structure, proton transport mechanism and function, ion selectivity of the M2A transmembrane peptide (residues 22−46) in the triply protonated His-37 state has been explored using multistate empirical valence bond simulations.[44,45] The computed permeation free energy profiles of excess proton and Na^+ along the +3 state of the channel[32] reveal a higher free energy barrier for Na^+ compared to the proton. However, no study (to our knowledge) has addressed the following questions on the unique properties of the M2A SF that confer proton selectivity; viz.,

(1) Although the M2A channel has a tetrameric $[His_4]^{2+}$ SF with two protonated and two neutral histidines at physiological pH, are all four histidines required and do two of the four histidines need to be protonated for proton selectivity; i.e., would the channel be as proton-selective if its oligomeric state were changed to say a trimer with a $[His_3]^{2+}$ SF or if less than or more than two histidines were protonated? In other words, does the tetrameric $[His_4]^{2+}$ SF in the M2A channel with two of the four histidines protonated at physiological pH have the best proton selectivity compared to other His protonation states or oligomeric states such as trimeric His filters?

DOI: 10.1021/jacs.6b08041
J. Am. Chem. Soc. 2016, 138, 13038−13047

(2) Although experiments show that replacing the histidines lining the M2A SF with other aa residues made the channel nonselective[13,15] (see above), how do mutations to nontitratable (backbone amide or Ser/Thr) or to other titratable (Asp/Glu) aa residues affect proton selectivity? For example, can Asp/Glu carboxylates in lieu of the SF histidines also accept a proton from an incoming H_3O^+?
(3) What are the physical principles governing the selectivity for proton over monovalent and divalent cations in the M2A SF?

Here, we endeavor to answer these questions by assessing how proton selectivity depends on various SF properties; namely, (1) its oligomeric state, (2) the protonation states of the SF residues, which determine the net charge q of the SF, (3) its solvent exposure, and (4) its ligand composition (i.e., His vs other ion-ligating groups). Our focus is on the SF and how its properties affect proton selectivity rather than the mechanism of channel opening and proton transport through the channel. As 3D structures are available only for the wild-type His_4^{2+} SF, we modeled M2A SFs varying in conformation, oligomericity, composition and net charge (see Table 1 and Methods) to gain insight into how these SF variables affect proton selectivity.

Table 1. Model M2A SFs Varying in Oligomericity, Conformation, Composition (SF residue type) and Charge

SF model	oligomeric state	SF residues[a]	SF charge q
$[\mathbf{His_3}]^q$	trimer	His^0, His^+	0, 1 or 2
$[\mathbf{His_4}]^{q,b}$ (His-box)	tetramer	His^0, His^+	0, 1, 2 or 3
$[\mathbf{His_4}]^{q,c}$ (Dimer-of-dimers)	tetramer	His^0, His^+	2
$[\mathbf{Bkb_4}]^0$	tetramer	$Backbone^0$	0
$[\mathbf{Ser_4}]^{2+}$	tetramer	Ser^0	0
$[\mathbf{Asp/Glu_4}]^{4-}$	tetramer	Asp^-/Glu^-	−4

[a]Superscripts denotes net charge of residue. [b]Starting conformation = "His-box" (Figure 1b). [c]Starting conformation = "Dimer-of-dimers" (Figure 1a).

The competition between protons and rival cations such as Na^+ in the various model SFs was evaluated by treating the interactions between the ion and SF ligands, which play a key role in the H_3O^+ vs Na^+ competition, explicitly using density functional theory; the region inside the SF was represented by an effective dielectric constant ε varying from 4 to 30 to mimic binding sites of increasing solvent exposure. Following Eisenman's equilibrium theory of ion selectivity,[46] the filter's selectivity can be expressed in terms of the free energy ΔG^x for replacing Na^+ bound inside a model SF, [Na^+-filter], with the "native" H_3O^+:

$$H_3O^+ + [Na^+\text{-filter}] \rightarrow [H_3O^+\text{-filter}] + Na^+ \quad (1)$$

The ion exchange free energy for eq 1 in an environment characterized by an effective dielectric constant $\varepsilon = x$ can be estimated as a sum of electronic (ΔG^1) and solvation ($\Delta\Delta G_{solv}{}^x$) effects:

$$\Delta G^x = \Delta G^1 + \Delta\Delta G_{solv}{}^x \quad (2)$$

where ΔG^1 is the gas−phase free energy for eq 1 and $\Delta\Delta G_{solv}{}^x$ is the difference in the solvation free energies $\Delta G_{solv}{}^x$ of the products and reactants in eq 1:

$$\Delta\Delta G_{solv}{}^x = \Delta G_{solv}{}^x([H_3O^+\text{-filter}]) + \Delta G_{solv}{}^x(Na^+) - \Delta G_{solv}{}^x([Na^+\text{-filter}]) - \Delta G_{solv}{}^x(H_3O^+) \quad (3)$$

Eq 2 thus allows us to isolate electronic effects (interactions between the SF and the permeating ion) from other effects such as the solvent accessibility and the effective dielectric constant in the filter, which are controlled by the protein matrix and membrane environment. A positive ΔG^x implies a Na^+-selective filter, whereas a negative value implies a H_3O^+-selective one. The above methodology has yielded trends in the free energy changes that are in line with experimental observations.[47−57] Hence, the calculations can yield reliable trends in the free energy changes with varying SF properties, but not accurate absolute binding free energies in the model SFs, which are thus not interpreted herein.

METHODS

Selectivity Filter Models. Since NMR[26,27] and crystallographic[28] studies reveal a tetrameric SF in the M2A protein channel lined with histidine residues, SFs containing four imidazole/imidazolium rings attached to a carbon−hydrogen ring scaffold via flexible methylene spacers were modeled (see Figure 1). Allowing a deprotonated His^0 to accept a proton, all possible combinations of protonation states for the other three histidine side chains lining the SF were modeled, resulting in $[His_4]^0$, $[His_4]^+$, $[His_4]^{2+}$, and $[His_4]^{3+}$ states. To study the effect of the channel's oligomericity on the H_3O^+/Na^+ competition, trimeric SFs containing different numbers of imidazole and imidazolium rings were also modeled, yielding $[His_3]^0$, $[His_3]^+$, and $[His_3]^{2+}$ SFs. Additionally, SFs containing four $-CONHCH_3$ (representing backbone peptide groups), −OH (representing the Ser side chains) and $-COO^-$ (representing the Asp^-/Glu^- side chains) groups were created to model mutant M2A SFs.

Models of the SFs were built using GaussView version 3.09,[58] following the guidelines from our previous work.[51] They were constructed on the basis of the following considerations:[51]

(a) The ring mimics the oligomeric state and overall symmetry of the ion channel pore.
(b) The ring scaffold prevents the metal ligands from drifting away or assuming unrealistic, pore-occluding positions during geometry optimization.
(c) The metal-ligating groups and their connection to the ring are flexible enough to allow them to optimize their positions upon cation binding.
(d) The shape and C−H orientations of the ring do not obstruct the pore lumen.

In most cases the proton was modeled as H_3O^+, but proton transfer reactions involving Zundel ($H_5O_2^+$) or Eigen ($H_9O_4^+$) type of ions were also considered (see Results). The M2A SF aperture has been found to be quite narrow[28] with a pore radius varying between 0.7 and 1.6 Å as the net charge of the histidines increased from 0 to 4.[41] Such a narrow pore is compatible with a dehydrated metal ion bound to the SF, thus we modeled a bare Na^+ inside the filter.

Gas-Phase Free Energy Calculations. Among several combinations of different ab initio/density functional theory methods (HF, MP2, S-VWN and B3-LYP) and basis sets (6-31+G(d,p), 6-31+G(2d,2p), 6-31+G(3d,p), 6-31+G(3d,2p), 6-311++G(d,p) and 6-311++G(3df,3pd)), the B3-LYP/6-31+G(3d,p) method has been shown to be the most efficient in yielding dipole moments of the SF ligands that are closest to the respective experimental values. It can also reproduce (within experimental error) the metal−oxygen bond distances in aqua and crown ether complexes, which resemble metal-occupied ion channel pores.[51] Hence, the B3-LYP/6-31+G(3d,p) method was used to optimize the geometry of each proton/metal complex and to compute the electronic energies, E_{el}, using the Gaussian 09 program.[59] During geometry optimization of the positively charged complexes, some of the imidazole/imidazolium

DOI: 10.1021/jacs.6b08041
J. Am. Chem. Soc. 2016, 138, 13038−13047

rings tended to flip away from the pore lumen due to charge repulsion and assumed unrealistic positions. To mimic the constraints imposed by the protein matrix on the movement of the SF ligands[41] and to preserve the integrity of the pore, the positions of the C$^{\gamma}$ carbon atoms (denoted by an asterisk in Figure 1b) of every imidazole/imidazolium ring were kept frozen during geometry optimization.

Frequency calculations for each optimized *trimeric* structure were performed at the same B3-LYP/6-31+G(3d,p) level of theory. Due to computer memory limitations, the smaller 6-31+G(d,p) basis set was used to compute the vibrational frequencies for the *tetrameric* structures. This would not be expected to affect the trends in the computed free energy changes, $\Delta G(H_3O^+ \rightarrow Na^+)$, as benchmark calculations on a trimeric SF with three imidazole ligating groups, $[His_3]^0$, revealed little change (<0.9 kcal/mol) in the thermal energy E_{th} and entropy S differences between H_3O^+-$[His_3]^0$ and Na^+-$[His_3]^0$ in going from the 6-31+G(3d,p) basis set (ΔE_{th} = 21.9 kcal/mol, $T\Delta S$ = 0.8 kcal/mol) to the smaller 6-31+G(d,p) basis set (ΔE_{th} = 22.0 kcal/mol, $T\Delta S$ = 1.7 kcal/mol). No imaginary frequency was found for the lowest energy conformation of any of the optimized structures. The frequencies were scaled by an empirical factor of 0.9613[60] and used to compute the thermal energies, including zero-point energy, and entropies.

The differences ΔE_{el}, ΔE_{th}, ΔPV (work term) and ΔS between the products and reactants in eq 1 were used to calculate the gas-phase ΔG^1 free energy at T = 298.15 K according to

$$\Delta G^1 = \Delta E_{el} + \Delta E_{th} + \Delta PV - T\Delta S \quad (4)$$

The basis set superposition error for an ion exchange reaction (such as eq 1) had been shown to be negligible,[51] and was thus not considered in the present calculations. Since electrostatic interactions dominate the energetics of cation−protein complexes,[61] dispersion interactions were found to make insignificant contributions (<1 kcal/mol) to the free energy of exchanging two cations;[62] thus, dispersion corrections were not included in the present evaluations.

Solution Free Energy Calculations. The ΔG_{solv}^{x} (x = 4, 10 or 30) values were estimated by solving Poisson's equation using finite difference methods[63,64] with the MEAD (Macroscopic Electrostatics with Atomic Detail) program,[65] as described in previous works.[66] Natural bond orbital atomic charges,[67] which are known to be numerically quite stable with respect to basis set changes, were employed in the calculations. The effective solute radii were obtained by adjusting the CHARMM (version 22)[68] van der Waals radii to reproduce the experimental hydration free energies of H_3O^+, Na^+, and model ligand molecules to within 1 kcal/mol (see Table 2). The resulting values (in Å) are R_H = 1.50, $R_H(H_3O^+)$ = 1.05, $R_H(NH_{imidazole})$ = 1.2, $R_H(NH_{imidazolium})$ = 1.1, R_C = 1.95, R_N = 1.75, $R_O(H_3O^+)$ = 1.65, $R_O(-CONHCH_3)$ = 1.72, $R_O(H_2O)$ = 1.85, $R_O(-CH_2OH)$ = 1.90, $R_O(-COO^-/-COOH)$ = 1.77, R_{Na} = 1.70.

Table 2. Comparison between Computed and Experimental pK_a and Hydration Free Energies, ΔG_{solv},[80] of Hydronium/Metal Cations and Ligands (in kcal/mol)

cation/ligand	expt	calcd	error[a]
	pK_a		
imidazole	6.7[b]	7.2	
	7.0[c]		
CH_3COOH	4.8[b,c]	4.9	
	ΔG_{solv}[80]		
H_3O^+	−108.0[d]	−108.8	−0.8
Na^+	−98.3[e]	−98.8	−0.5
H_2O	−6.3[f]	−6.7	−0.4
$HCONH_2$	−10.0[g]	−10.6	−0.6
CH_3OH	−5.1[h]	−6.1	−1.0
CH_3COOH	−6.7[i]	−6.7	0.0
Imidazole	−10.2[i]	−11.0	−0.8

[a]Error = ΔG_{solv}[80](Calcd) − ΔG_{solv}[80](Expt). [b]From Pearson, 1986.[69] [c]From Smith et al., 1989.[70] [d]From Kelly et al., 2005[71] [e]From Friedman and Krishnan, 1973.[72] [f]From Ben-Naim annd Marcus, 1984.[73] [g]From Wolfenden, 1978.[74] [h]From Chambers et al., 1996.[75] [i]From Wolfenden et al., 1981.[76]

RESULTS

The $[His_4]^{2+}$ Model SFs Resemble the M2A SFs. Following experimental observation, two models of M2A SFs were designed to mimic the "dimer-of-dimers" (2L0J; Figure 1a) and "His-box" (3LBW; Figure 1b) structures. Both models contain a pair of protonated imidazole rings and a pair of deprotonated imidazoles yielding a dicationic $[His_4]^{2+}$ construct at ambient pH. They differ in the mutual arrangement of the His rings depending on the SF conformation. For the "dimer-of-dimers" SF, a model comprising two pairs of hydrogen-bonded rings, involving an imidazolium N−H donating a hydrogen bond to the imidazole N_δ as seen in the 2L0J structure, was optimized. The resultant structure (Figure 1a, right) exhibits good overall agreement with the experimentally observed structure: the mean N−H···N_δ hydrogen bond distance (1.94 Å) is similar to the respective experimental value (1.86 Å). For the other model, the optimized structure shows two neutral imidazole rings deprotonated at the N_ε atom and an assembly of the His rings resembling the "His-box" in the 3LBW crystal structure (Figure 1b), where the rings are nearly perpendicular to each other. Moreover, the size of the "His-box" in these two structures, measured by the distances between the four Cγ atoms (indicated by asterisks in Figure 1b), are very similar: the cross section of the "His-box" in the X-ray structure is 5.6 × 5.6 Å, whereas that in the optimized SF structure is 5.1 × 5.4 Å.

Binding of H_3O^+ to Dimer-of-Dimer and His-box SF Conformations. The two $[His_4]^{2+}$ SF models were tested for their ability to bind to the cognate H_3O^+. Figure 2 shows the initial and fully optimized structures of the two H_3O^+-$[His_4]^{2+}$ complexes. Both SF conformations behave similarly with respect to coordinating and deprotonating H_3O^+: In the fully optimized structures, the incoming H_3O^+ protonated one of the SF imidazoles, which formed a hydrogen bond with the residual water molecule along with the other imidazole and an imidazolium, whereas the second imidazolium ring flips outward slightly in response to the increased positive charge density in the binding site. Consequently, the hydrogen-bond pair characteristic of the "dimer-of-dimers" SF structure is disrupted upon binding H_3O^+ (Figure 2a, right). Binding of H_3O^+ to the $[His_4]^{2+}$ "dimer-of-dimers" or "His-box" conformation not only resulted in similar overall structures, but also yielded virtually isoenergetic complexes whose electronic energies differ by only 0.7 kcal/mol. These results imply that the two SF conformations achieve essentially the same "conductive"-state structure regardless of their initial conformation and the site of His ring protonation (N_δ for "dimer-of-dimers" and N_ε for the "His-box" SF). Since the "His-box" construct formed a slightly more stable complex with H_3O^+ than its "dimer-of-dimers" counterpart, it was used in the analyses below.

Proton Transfer to $[His_4]^{2+}$ SF. In aqueous solution, the proton exists as aqua complexes with varying numbers of water molecules. Apart from hydronium (H_3O^+), the most frequently observed structures are Zundel ($H_5O_2^+$) and Eigen ($H_9O_4^+$) cations.[77−79] Can these bulkier species protonate the M2A SF in its resting $[His_4]^{2+}$ configuration like the hydronium? To address this, the structures of the $[His_4]^{2+}$ SF bound to $H_5O_2^+$

DOI: 10.1021/jacs.6b08041
J. Am. Chem. Soc. 2016, 138, 13038−13047

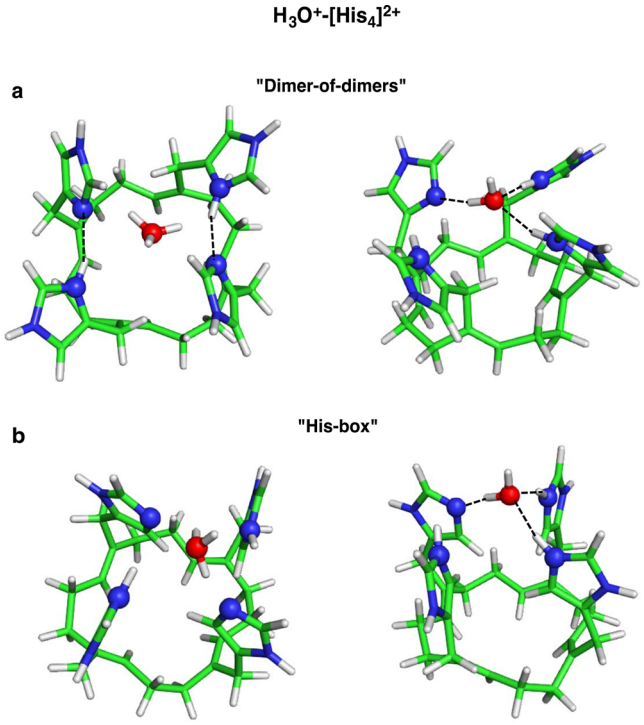

Figure 2. Initial (left) and final optimized (right) structures of H_3O^+ bound to $[His_4]^{2+}$ SF in (a) "dimer-of-dimers" and (b) "His-box" conformation. The ΔG^1, ΔG^4, and ΔG^{30} are 43, 18, and 14 kcal/mol, respectively, for proton binding to the "dimer-of-dimers" conformation and 22, −1, and −3 kcal/mol, respectively, for proton binding to "His-box" conformation. These absolute H_3O^+ binding free energies are less reliable than the H_3O^+ and Na^+ binding free energy differences (eq 1) in Figures 4−6, and were thus not interpreted.

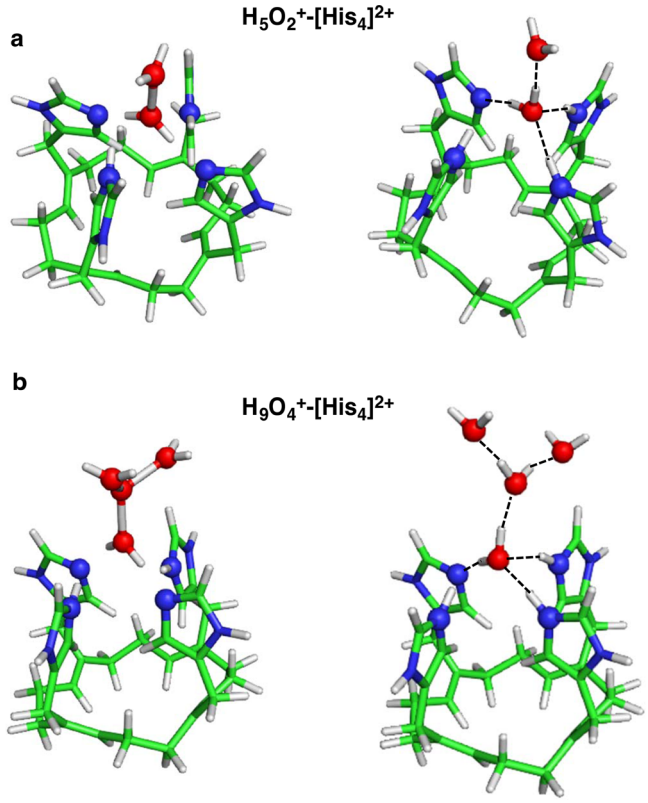

Figure 3. Initial (left) and final optimized (right) structures of complexes between $[His_4]^{2+}$ SFs and (a) $H_5O_2^+$, and (b) $H_9O_4^+$ ions.

and $H_9O_4^+$ ions were optimized. In both cases, a proton from the incoming cationic species (Figure 3, left) was spontaneously transferred to one of the imidazole rings (Figure 3, right), resulting in a nonbonded complex between the triply protonated $[His_4]^{3+}$ SF and water molecule(s). A network of hydrogen bonds between the SF and water molecules as well as between water molecules in the Zundel or Eigen species stabilized the complex. These results along with those from Figure 2 (see above) are in line with experimental and other theoretical findings[24,26,35,38,40−43] suggesting that a neutral His residue can accept the incoming proton, despite the high positive charge of the M2A SF. Since H_3O^+, $H_5O_2^+$ and $H_9O_4^+$ ions behaved similarly in protonating the model SF and frequency calculations of the *tetrameric* structures were already computationally prohibitive, reactions with H_3O^+ were considered for the rest of the study.

H_3O^+/Na^+ Selectivity in Trimeric His_3 and Tetrameric His_4 SFs. To assess the role of the M2A SF's (i) overall charge, (ii) solvent exposure, and (iii) oligomericity in the competition between H_3O^+ and Na^+, trimeric and tetrameric SFs containing different combinations of protonated and deprotonated imidazole rings bound to H_3O^+ and Na^+ were optimized; the resulting structures were used to compute the free energy ΔG^x for replacing Na^+ bound inside the model SF with the "native" H_3O^+. Regardless of the His protonation states, both trimeric (Figure 4, right) and tetrameric (Figure 5, right) SFs can abstract a proton from the approaching hydronium ion. This increases the overall SF charge and thus electrostatic repulsion among the positively charged SF histidines, which is partially compensated by a network of stabilizing hydrogen bonds formed by the water molecule to both the free imidazole N and/or protonated imidazolium H(N).

Increasing the SF Positive Charge up to +2e Increases H_3O^+/Na^+ Selectivity. This tendency is clearly demonstrated by the ion exchange free energies in Figures 4 and 5. As the positive charge increases in going from the $[His_3]^0$ to $[His_3]^+$ to $[His_3]^{2+}$ trimeric SF, the free energy for replacing Na^+ in the trimeric filter with H_3O^+ becomes more favorable in the gas phase (ΔG^1 decreased from −14 to −30 to −39 kcal/mol) and in a protein environment ($\Delta G^4/\Delta G^{30}$ decreased from −10/−6 to −19/−11 to −23/−13 kcal/mol). The same trend was found for the tetrameric $[His_4]^0$, $[His_4]^+$, and $[His_4]^{2+}$ SFs where the ΔG^1 decreased from −21 to −32 to −50 kcal/mol, while the ΔG^{30} decreased from −14 to −16 to −27 kcal/mol. Increasing the SF charge from 0 to +2e makes the filter less accommodating to the incoming Na^+ due to the increased repulsion among the increasing number of positively charged histidines and Na^+ combined with the lack of stabilizing interactions found in the hydronium complexes.

For the tetrameric filters, increasing the positive charge beyond +2 did not further increase proton selectivity, which in fact, decreased: The gas-phase ΔG^1 free energy for $[His_4]^{3+}$ (−46 kcal/mol, Figure 5d) is less favorable than that for $[His_4]^{2+}$ (−50 kcal/mol, Figure 5c). This is probably because proton transfer from H_3O^+ to the $[His_4]^{3+}$ SF yields four positively charged His^+, whose repulsive interactions are stronger and less well compensated than those among the three positively charged His^+ and H_2O: the water molecule interacts with only one histidine in the $[His_4]^{3+}$ filter (Figure 5d), but with three histidines in the $[His_4]^{2+}$ filter (Figure 5c).

DOI: 10.1021/jacs.6b08041
J. Am. Chem. Soc. 2016, 138, 13038−13047

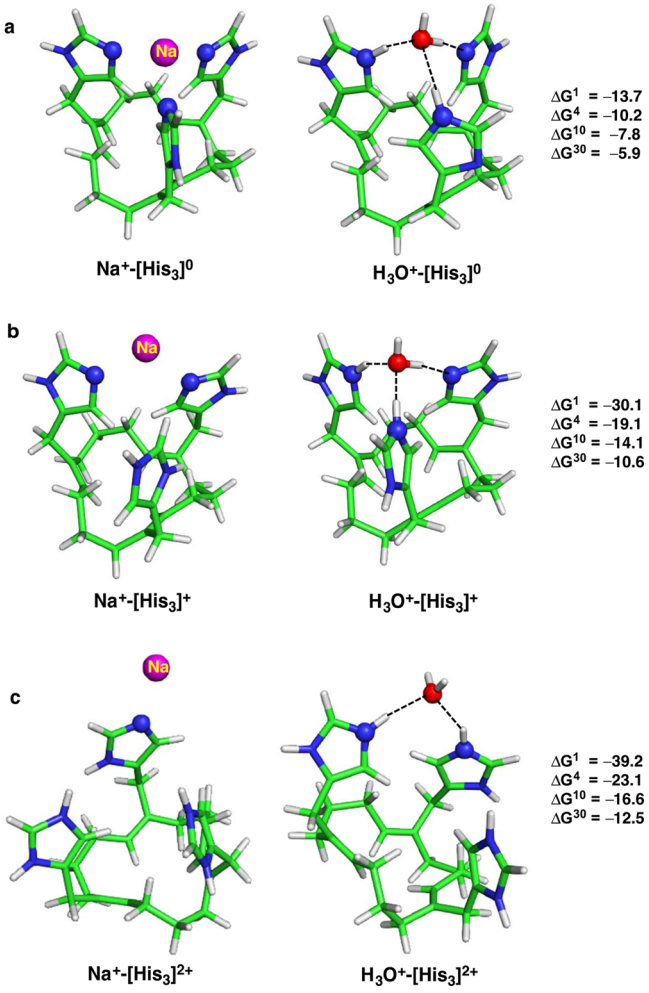

Figure 4. B3-LYP/6-31+G(3d,p) optimized structures of Na^+ and H_3O^+-bound to model *trimeric* SFs lined with imidazole/imidazolium groups: (a) $[His_3]^0$, (b) $[His_3]^+$, and (c) $[His_3]^{2+}$. The free energies ΔG^x (in kcal/mol) for replacing Na^+ in the SF characterized by dielectric constant $\varepsilon = x$ with H_3O^+ are shown on the right. ΔG^1 refers to cation exchange free energy in the gas phase, whereas ΔG^4, ΔG^{10} and ΔG^{30} refer to cation exchange free energies in an environment characterized by an effective dielectric constant of 4, 10 and 30, respectively.

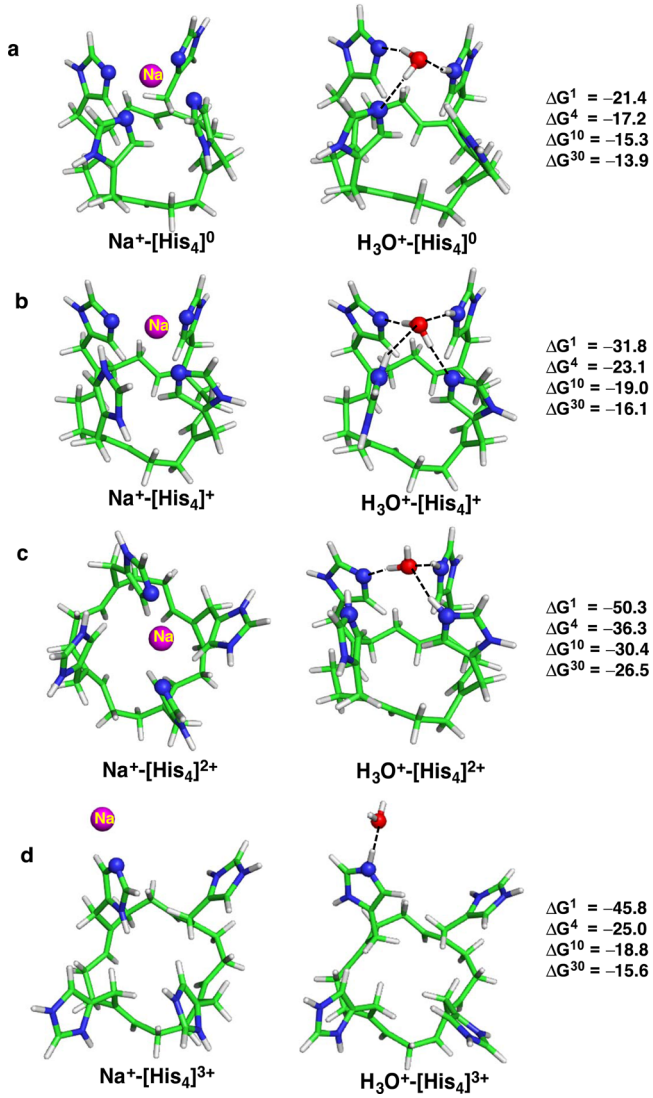

Figure 5. B3-LYP/6-31+G(3d,p) optimized structures of Na^+ and H_3O^+-bound to model *tetrameric* SFs lined with imidazole/imidazolium groups: (a) $[His_4]^0$, (b) $[His_4]^+$, (c) $[His_4]^{2+}$, and (d) $[His_4]^{3+}$. The free energies ΔG^x (in kcal/mol) for replacing Na^+ in the SF characterized by dielectric constant $\varepsilon = x$ with H_3O^+ are shown on the right. ΔG^1 refers to cation exchange free energy in the gas phase, whereas ΔG^4, ΔG^{10} and ΔG^{30} refer to cation exchange free energies in an environment characterized by an effective dielectric constant of 4, 10 and 30, respectively.

Decreasing the SF Solvent Exposure Increases H_3O^+ Selectivity. Interestingly, both trimeric and tetrameric filters appear to be H_3O^+/Na^+ selective over the entire dielectric range from ε = 4 to 30 (negative ΔG^x in Figures 4 and 5). However, solvent-inaccessible His filters were found to be more H_3O^+/Na^+-selective than their solvent exposed counterparts (ΔG^4 is more negative than ΔG^{30} in Figures 4 and 5). Increasing the solvent exposure of the SF increased the ion exchange free energies ΔG^x for all the His filters, as the desolvation penalty of the incoming H_3O^+ outweighed the solvation free energy gain of the outgoing Na^+ (see eq 1).

Tetrameric His_4 SFs Are More Proton-Selective than Trimeric Ones. The $[His_4]^q$ (q = 0, 1, or 2) filter in Figure 5 has a more favorable $H_3O^+ \rightarrow Na^+$ free energy than the corresponding $[His_3]^q$ filter with the same net charge q in Figure 4. The enhanced proton selectivity in *tetrameric* SFs can be attributed to the combined effects of two factors: Increasing the metal coordination from three to four increases the steric repulsion among the bulky protein ligands around Na^+;[52] thus a tetrameric His_4 SF would be expected to be less competitive in binding Na^+ than its trimeric counterpart. At the same time, a *tetrameric* His_4 SF provides a better environment for binding H_3O^+ compared to a *trimeric* one with the same net charge by enabling a more elaborate hydrogen-bonding network (e.g., compare Figures 5c with 4c). Notably among all the His filters examined, the $[His_4]^{2+}$ SF, which models the M2A filter at a resting state, exhibits the highest proton selectivity (most negative ΔG^x) over the entire dielectric range from 1 to 30.

H_3O^+/Na^+ Selectivity in Tetrameric SFs Lined with Backbones, Ser, Asp/Glu Residues. Can SFs lined with aa residues other than histidines be selective for protons? To answer this question, we modeled H_3O^+ and Na^+ complexes of homotetrameric SFs lined with backbone groups ($-CONHCH_3$), Ser side chains ($-OH$), or Asp^-/Glu^- side chains (COO^-).

DOI: 10.1021/jacs.6b08041
J. Am. Chem. Soc. 2016, 138, 13038–13047

Tetrameric Ser/Backbone$_4$ SFs Are Not Proton-Selective. Filters lined with nontitratable groups such as backbone peptide groups (Figure 6a) or Ser side chains (Figure 6b) are

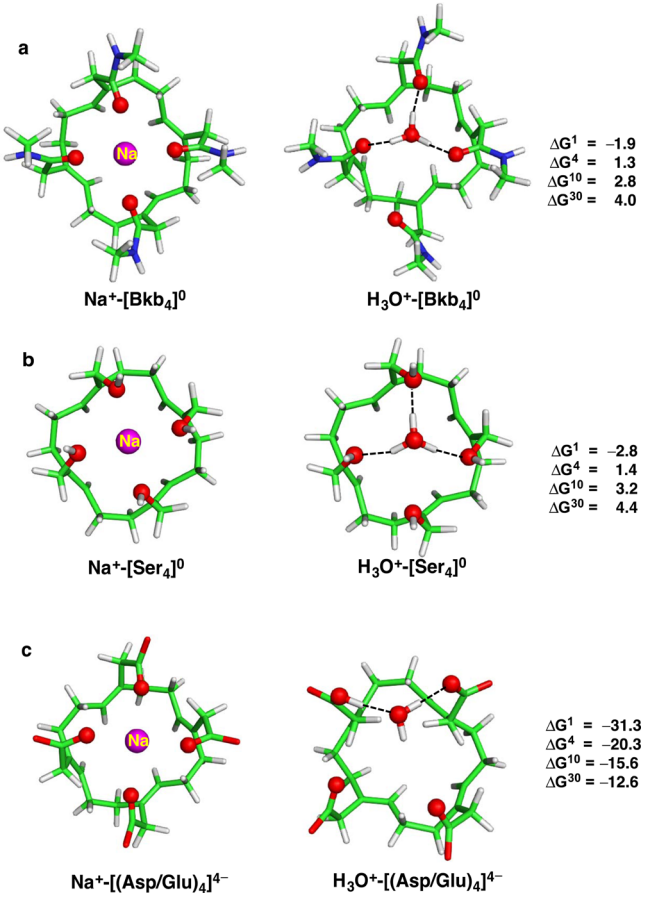

Figure 6. B3-LYP/6-31+G(3d,p) optimized structures of Na^+ and H_3O^+-bound to model *tetrameric* SFs lined with (a) amide, $[Bkb_4]^0$, (b) hydroxyl, $[Ser_4]^0$ and (c) carboxyl, $[(Asp/Glu)_4]^{4-}$ groups. The free energies ΔG^x (in kcal/mol) for replacing Na^+ in the SF characterized by dielectric constant $\varepsilon = x$ with H_3O^+ are shown on the right. ΔG^1 refers to cation exchange free energy in the gas phase, whereas ΔG^4, ΔG^{10} and ΔG^{30} refer to cation exchange free energies in an environment characterized by an effective dielectric constant of 4, 10 and 30, respectively.

not proton-selective: The $H_3O^+ \rightarrow Na^+$ free energies, ΔG^x ($x \geq 4$), are all positive. This is because the ligating oxygen atoms from the $[Bkb_4]^0$ and $[Ser_4]^0$ filters have weaker interactions with H_3O^+ and cannot deprotonate it, compared with the imidazole nitrogen atoms from the $[His_4]^0$ filter, which can deprotonate H_3O^+. Furthermore, these "hard" (weakly polarizable) oxygen-containing ligands interact more favorably with the "hard" Na^+ cation, compared with the less "hard" nitrogen atoms from the $[His_4]^0$ filter. Hence, the $H_3O^+ \rightarrow Na^+$ gas-phase free energy ΔG^1 for the $[Bkb_4]^0$ or $[Ser_4]^0$ filter (−2 or −3 kcal/mol) is less favorable than that for the $[His_4]^0$ filter (−21 kcal/mol) and cannot offset the unfavorable solvation effects, resulting in positive ΔG^x (x = 4 to 30).

Tetrameric Asp/Glu$_4$ SFs Are H_3O^+/Na^+-Selective, but Are Even More Ca^{2+}-Selective. In contrast to the nonproton-selective $[Bkb_4]^0$ and $[Ser_4]^0$ filters, a tetra-anionic $[(Asp/Glu)_4]^{4-}$ SF lined with four titratable Asp^- or Glu^- residues is predicted to be H_3O^+/Na^+ selective (negative ΔG^x, x = 1 to 30, Figure 6c). A $[(Asp/Glu)_4]^{4-}$ SF could act as a relay switch in proton translocation by extracting a proton from the H_3O^+ to one of the carboxylate ligand, in analogy to the neutral histidine in His_3 or His_4 SFs. The $[(Asp/Glu)_4]^{4-}$ SF, however, is much less selective for protons ($\Delta G^4/\Delta G^{30}$ = −20/−13 kcal/mol, Figure 6c) than the "native" $[His_4]^{2+}$ SF ($\Delta G^4/\Delta G^{30}$ = −36/−26 kcal/mol, Figure 5c). This is probably because monocationic Na^+ binds more favorably to the negatively charged $[(Asp/Glu)_4]^{4-}$ filter than to the positively charged $[His_4]^{2+}$ filter.

Although a $[(Asp/Glu)_4]^{4-}$ filter could be selective for H_3O^+/Na^+, it would not be selective for H_3O^+ over all other contenders in the extracellular fluids, in particular divalent Ca^{2+}: The free energies for replacing Ca^{2+} in the $[(Asp/Glu)_4]^{4-}$ filter with H_3O^+ in the gas-phase is highly unfavorable (407 kcal/mol) and remains quite unfavorable even if the site were solvent-accessible (ΔG^{30} = 44 kcal/mol). Thus, the $[(Asp/Glu)_4]^{4-}$ filter does not appear to be functional in selecting protons over the entire set of competing cationic species present in the surrounding fluids. In fact, four Asp/Glu side chains lining a narrow SF that can fit dehydrated or monohydrated Ca^{2+} is the signature of SFs in Ca^{2+}-selective voltage-gated ion channels.[61,80]

DISCUSSION

Previous experimental and theoretical studies have focused on the mechanism of ion transport through the M2A channel rather than the properties of its conserved His_4 SF that controls proton selectivity. Here, we have delineated the physical principles controlling proton selectivity in SFs lined with histidines by determining the thermodynamic outcome of the H_3O^+ vs Na^+ competition in model SFs differing in oligomericity, His tetrad protonation/charge state, effective dielectric environment, and ligand composition. Note that the His protonation state and the effective dielectric environment of the SF can be modulated by the protein matrix. Hence, although protein regions outside the SF have not been modeled explicitly, some of their effects on ion binding to the His tetrad have been taken into account by examining how the computed free energies change with varying SF net charge and solvent accessibility. Although we have used a reduced SF model to assess how the different SF properties affect proton selectivity, the trends in the $H_3O^+ \rightarrow Na^+$ free energies are, nevertheless, in line with available experimental observations (see below). They help to elucidate the selectivity properties of M2A wild-type channel SF and some of its mutant variants.

Comparison with Experiment. The optimized structures of the $[His_4]^{2+}$ SFs modeling the M2A SFs in their resting state closely resemble the "dimer-of-dimers" structure (PDB entry 2L0J, Figure 1a) and "His-box" structure revealed by NMR (PDB entry 2RLF) and X-ray crystallography (PDB entry 3LBW; Figure 1b). Interestingly, these two $[His_4]^{2+}$ SF conformations ("His-box" and "dimer-of-dimers") converge to nearly identical "conductive"-state structures upon binding H_3O^+ (Figure 2). In line with experimental observations,[20,24,40] the $[His_4]^{2+}$ model SF has high proton affinity and can easily be protonated by the incoming proton existing as H_3O^+, $H_5O_2^+$, or $H_9O_4^+$ (Figures 2 and 3). Our calculations are consistent with experimental studies showing that protonation of a third histidine resulting in a $[His_4]^{3+}$ SF triggers proton permeation through the channel.[6,18,19] Whereas a H_3O^+ binds roughly in the plane of the $[His_4]^{2+}$ SF ring and interacts with three of the histidines (Figure 5c), it is ejected from the $[His_4]^{3+}$ SF plane, interacting with only one of the four histidines (Figure 5d).

DOI: 10.1021/jacs.6b08041
J. Am. Chem. Soc. 2016, 138, 13038−13047

That a solvent-accessible His_4 SF is H_3O^+/Na^+-selective (Figure 5c) is consistent with NMR[24,37] and X-ray[81] data indicating an aqueous pore with the His tetrad in contact with water.

The results of the mutant M2A SFs also agree with experimental findings: They agree with mutagenesis studies[15] showing that mutating His-37 in the M2A SF to a neutral aa residue such as Gly, Ser, or Thr made the channel nonselective: the mutant tetrameric SFs lined with backbone amide groups (Figure 6a) or serine hydroxyl groups (Figure 6b) are not proton-selective (positive ΔG^x, $x \geq 4$). They also agree with experimental studies showing that voltage-gated sodium channels possessing SFs with four acidic residues are, indeed, selective for H_3O^+ over Na^+ at low pH.[82−85]

Factors Governing Proton Selectivity in the M2A SFs. Most studies support a proton-relay mechanism for proton conductivity in both the M2A[24,26,35,38,40−43] and the voltage-gated H_v1[5,57] channels, underscoring the role of a titratable residue (His in the former and Asp^- in the latter) in relaying a proton from one side of the filter to the other. Our results, which are summarized in Figure 7, reveal that the availability of

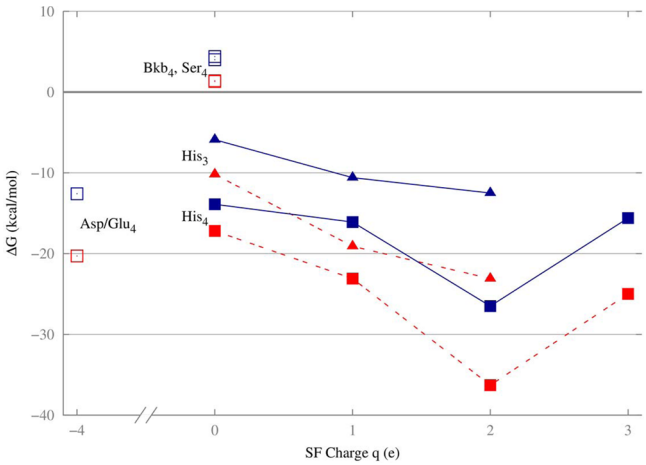

Figure 7. Plot of the ΔG^4 (red) and ΔG^{30} (blue) in Figures 4−6 as a function of the SF net charge. Filled triangles and squares denote His_3 and His_4 SFs, respectively, while open squares denote tetrameric mutant SFs. The dashed and solid lines connect the ΔG^4 and ΔG^{30} values, respectively, for the His_3 and His_4 SFs in Figures 4 and 5. $\Delta G^x > 0$ indicates a Na^+-selective SF, whereas $\Delta G^x < 0$ implies a H_3O^+-selective one.

a titratable residue in the SF that can serve as a proton acceptor is crucial not only for the channel's conductivity, but also for its selectivity: Among all types of SFs examined herein, those containing nontitratable aa residues ($[Bkb_4]^0$ and $[Ser_4]^0$) were found to be nonproton-selective (positive ΔG^x, $x \geq 4$, Figure 7). On the other hand, SFs comprising titratable His or Asp^-/Glu^- residues that can deprotonate the incoming H_3O^+ were found to be H_3O^+/Na^+-selective over the entire dielectric range from 1 to 30 (negative ΔG^x, Figure 7). Our results also reveal that the protein matrix could play an important role in governing the protonation state of the SF histidines: Increasing the number of the protonated histidines in the pore up to two, which increases the SF net charge from 0 to +2, favors H_3O^+ over Na^+. In addition, increasing the channel protein's oligomericity from three to four also enhances proton selectivity.

Considering the SF's oligomericity, solvent exposure, ligand composition and charge/ionization state, the combination that was found to yield the best thermodynamic H_3O^+/Na^+ selectivity is the $[His_4]^{2+}$ structure, as shown in Figure 7: In the series of trimeric and tetrameric structures, the $[His_4]^{2+}$ filter comprising two positively charged imidazolium rings has the highest H_3O^+/Na^+ selectivity. Coincidentally, this $[His_4]^{2+}$ structure represents the "native" M2A SF in its resting state. Thus, it appears that the set of physical principles outlined above has been optimized during evolution to yield a tetrameric filter comprising titratable His residues with a net charge of +2 to maximize the performance of the M2A channel.

Proton Selectivity of the $[His_4]^{2+}$ SF via Suboptimal Binding of Rival Cations. It has been suggested that Na^+ and K^+ are prohibited from entering the $[His_4]^{2+}$ SF pore due to the size of the four imidazole side chains lining the filter, which obstructs the pore.[18] In contrast, our results show that Na^+ can bind to the $[His_4]^{2+}$ SF, but not as well as H_3O^+: Compared with a trimeric filter, a larger tetrameric pore provides a less favorable environment for binding Na^+, which prefers a coordination number of three rather than four,[52] but better conditions for binding H_3O^+, which can form more stabilizing interactions than in a trimeric filter. Furthermore, compared with a neutral $[His_4]^0$ or monocationic $[His_4]^+$ filter, a dicationic $[His_4]^{2+}$ pore disfavors binding of cations such as Na^+, K^+, or Ca^{2+} due to the strong repulsive forces among the positively charged entities and the lack of stabilizing hydrogen-bonding interactions between the non-native cation and the filter.

Limitations and Future Work. Because our focus is on the SF, we have resorted to a reduced SF model that treated interactions between the ion and SF ligands accurately using density functional theory and interactions with the other nonSF residues implicitly. Another limitation is that ion selectivity of the various model SFs was based on the binding free energy difference between hydronium and Na^+; however, different kinetic barriers for the two ions could also contribute to ion selectivity. Our finding that Na^+ binds less well to the wild-type $[His_4]^{2+}$ SF than H_3O^+ complements previous simulations showing that Na^+ encounters a larger free energy barrier at the $[His_4]^{3+}$ SF than H_3O^+.[32] When accurate structures of M2A with the mutant SFs modeled herein become available, it would be interesting to compute ion permeation free profiles, as obtained for the wild-type $[His_4]^{3+}$ SF.[32,33] A combination of various methodologies (e.g., the approach herein, classical, reactive, and ab initio molecular dynamics simulations, QM/MM simulations) focusing on various properties of the M2A channel integrated with experimental studies would hopefully provide an in-depth understanding of M2A channel gating, proton transport, and proton selectivity mechanisms, which in turn would help guide the design of new anti-influenza agents.

■ ASSOCIATED CONTENT

Supporting Information

The Supporting Information is available free of charge on the ACS Publications website at DOI: 10.1021/jacs.6b08041.

Electronic energies and Cartesian coordinates of the fully optimized B3LYP/6-31+G(3d,p) structures of model SFs (PDF)

DOI: 10.1021/jacs.6b08041
J. Am. Chem. Soc. 2016, 138, 13038−13047

AUTHOR INFORMATION

Corresponding Authors

*t.dudev@chem.uni-sofia.bg

*carmay@gate.sinica.edu.tw

Notes

The authors declare no competing financial interest.

ACKNOWLEDGMENTS

This work was supported by Academia Sinica and the Ministry of Science and Technology in Taiwan.

REFERENCES

(1) Wang, C.; Lamb, R. A.; Pinto, L. H. *Virology* **1994**, *205*, 133.

(2) Lamb, R. A.; Holsinger, L. J.; Pinto, L. H. In *Receptor-Mediated Virus Entry into Cells*; Wimmer, E., Ed.; Cold Spring Harbor Press: Cold Spring Harbor, NY, 1994; p 303.

(3) Lamb, R. A.; Zebedee, S. L.; Richardson, C. D. *Cell* **1985**, *40*, 627.

(4) Wang, J.; Li, F.; Ma, C. *Biopolymers* **2015**, *104*, 291.

(5) DeCoursey, T. E.; Hosler, J. *J. R. Soc., Interface* **2014**, *11*, 20130799.

(6) Chizhmakov, I. V.; Geraghty, F. M.; Ogden, D. C.; Hayhurst, A.; Antoniou, M.; Hay, A. J. *J. Physiol.* **1996**, *494*, 329.

(7) Mould, J. A.; Li, H. C.; Dudlak, C. S.; Lear, J. D.; Pekosz, A.; Lamb, R. A.; Pinto, L. H. *J. Biol. Chem.* **2000**, *275*, 8592.

(8) Lin, T. I.; Schroeder, C. *J. Virol.* **2001**, *75*, 3647.

(9) Chizhmakov, I. V.; Ogden, D. C.; Geraghty, F. M.; Hayhurst, A.; Skinner, A.; Betakova, T.; Hay, A. J. *J. Physiol.* **2003**, *546.2*, 427.

(10) Moffat, J. C.; Vijayvergiya, V.; Gao, P. F.; Cross, T. A.; Woodbury, D. J.; Busath, D. D. *Biophys. J.* **2008**, *94*, 434.

(11) Leiding, T.; Wang, J.; Martinsson, J.; DeGrado, W. F.; Årsköld, S. P. *Proc. Natl. Acad. Sci. U. S. A.* **2010**, *107*, 15409.

(12) Peterson, E.; Ryser, T.; Funk, S.; Inouye, D.; Sharma, M.; Qin, H.; Cross, T. A.; Busath, D. D. *Biochim. Biophys. Acta, Biomembr.* **2011**, *1808*, 516.

(13) Wang, C.; Lamb, R. A.; Pinto, L. H. *Biophys. J.* **1995**, *69*, 1363.

(14) Shuck, K.; Lamb, R. A.; Pinto, L. H. *J. Virol.* **2000**, *74*, 7755.

(15) Venkataraman, P.; Lamb, R. A.; Pinto, L. H. *J. Biol. Chem.* **2005**, *280*, 21463.

(16) Tang, Y.; Zaitseva, F.; Lamb, R. A.; Pinto, L. H. *J. Biol. Chem.* **2002**, *277*, 39880.

(17) Ito, T.; Gorman, O. T.; Kawaoka, K.; Bean, W. J.; Webster, R. G. *J. Virol.* **1991**, *65*, 5491.

(18) Pinto, L. H.; Lamb, R. A. *J. Biol. Chem.* **2006**, *281*, 8997.

(19) Hu, J.; Fu, R.; Nishimura, K.; Zhang, L.; Zhou, H. X.; Busath, D. D.; Vijayvergiya, V.; Cross, T. A. *Proc. Natl. Acad. Sci. U. S. A.* **2006**, *103*, 6865.

(20) Hu, F.; Schmidt-Rohr, K.; Hong, M. *J. Am. Chem. Soc.* **2012**, *134*, 3703.

(21) Colvin, M. T.; Andreas, L. B.; Chou, J. J.; Griffin, R. G. *Biochemistry* **2014**, *53*, 5987.

(22) Liao, S. Y.; Yang, Y.; Tietze, D.; Hong, M. *J. Am. Chem. Soc.* **2015**, *137*, 6067.

(23) Yimin Miao, R. F.; Zhou, H.-X.; Cross, T. A. *Structure* **2015**, *23*, 2300.

(24) Hong, M.; Fritzsching, K. J.; Williams, J. K. *J. Am. Chem. Soc.* **2012**, *134*, 14753.

(25) Zhou, H. X.; Cross, T. *Protein Sci.* **2013**, *22*, 381.

(26) Sharma, M.; Yi, M.; Dong, H.; Qin, H.; Peterson, E.; Busath, D.; Zhou, H.; Cross, T. *Science* **2010**, *330*, 509.

(27) Schnell, J. R.; Chou, J. J. *Nature* **2008**, *451*, 591.

(28) Acharya, R.; Carnevale, V.; Fiorin, G.; Levine, B. G.; Polishchuk, A. L.; Balannik, V.; Samish, I.; Lamb, R. A.; Pinto, L. H.; DeGrado, W. F.; Klein, M. L. *Proc. Natl. Acad. Sci. U. S. A.* **2010**, *107*, 15075.

(29) Sansom, M. S. P.; Kerr, I. D.; Smith, G. R.; Son, H. S. *Virology* **1997**, *233*, 163.

(30) Okada, A.; Miura, T.; Takeuchi, H. *Biochemistry* **2001**, *40*, 6053.

(31) Smondyrev, A. M.; Voth, G. A. *Biophys. J.* **2002**, *82*, 1460.

(32) Chen, H.; Wu, Y.; Voth, G. A. *Biophys. J.* **2007**, *93*, 3470.

(33) Liang, R.; Li, H.; Swanson, J. M. J.; Voth, G. A. *Proc. Natl. Acad. Sci. U. S. A.* **2014**, *111*, 9396.

(34) Pinto, L. H.; Dieckmann, G. R.; Gandhi, C. S.; Papworth, C. G.; Braman, J.; Shaughnessy, M. A.; Lear, J. D.; Lamb, R. A.; DeGrado, W. F. *Proc. Natl. Acad. Sci. U. S. A.* **1997**, *94*, 11301.

(35) Lear, J. D. *FEBS Lett.* **2003**, *552*, 17.

(36) Carnevale, V.; Fiorin, G.; Levine, B. G.; DeGrado, W. F.; Klein, M. L. *J. Phys. Chem. C* **2010**, *114*, 20856.

(37) Hu, F.; Luo, W.; Hong, M. *Science* **2010**, *330*, 505.

(38) Phongphanphanee, S.; Rungrotmongkol, T.; Yoshida, N.; Hannongbua, S.; Hirata, F. *J. Am. Chem. Soc.* **2010**, *132*, 9782.

(39) Pielak, R. M.; Chou, J. J. *J. Am. Chem. Soc.* **2010**, *132*, 17695.

(40) Zhou, H. X. *J. Membr. Biol.* **2011**, *244*, 93.

(41) Wei, C.; Pohorille, A. *Biophys. J.* **2013**, *105*, 2036.

(42) Dong, H.; Yi, M.; Cross, T. A.; Zhou, H. X. *Chem. Sci.* **2013**, *4*, 2776.

(43) Polishchuk, A. L.; Cristian, L.; Pinto, L. H.; Lear, J. D.; DeGrado, W. F. *Biochim. Biophys. Acta, Biomembr.* **2014**, *1828*, 1082.

(44) Swanson, J. M.; Maupin, C. M.; Chen, H.; Petersen, M. K.; Xu, J.; Wu, Y.; Voth, G. A. *J. Phys. Chem. B* **2007**, *111*, 4300.

(45) Wu, Y.; Chen, H.; Wang, F.; Paesani, F.; Voth, G. A. *J. Phys. Chem. B* **2008**, *112*, 467.

(46) Eisenman, G. In *Symposium on Membrane Transport and Metabolism*; Kleinzeller, A., Kotyk, A., Eds.; Academic Press: New York, 1961; p 163.

(47) Dudev, T.; Lim, C. *J. Phys. Chem. B* **2001**, *105*, 4446.

(48) Babu, C. S.; Dudev, T.; Casareno, R.; Cowan, J. A.; Lim, C. *J. Am. Chem. Soc.* **2003**, *125*, 9318.

(49) Dudev, T.; Lim, C. *J. Phys. Chem. B* **2004**, *108*, 4546.

(50) Dudev, T.; Chang, L.-Y.; Lim, C. *J. Am. Chem. Soc.* **2005**, *127*, 4091.

(51) Dudev, T.; Lim, C. *J. Am. Chem. Soc.* **2009**, *131*, 8092.

(52) Dudev, T.; Lim, C. *J. Am. Chem. Soc.* **2010**, *132*, 2321.

(53) Dudev, T.; Lim, C. *J. Am. Chem. Soc.* **2011**, *133*, 9506.

(54) Dudev, T.; Lim, C. *J. Am. Chem. Soc.* **2013**, *135*, 17200.

(55) Dudev, T.; Lim, C. *J. Am. Chem. Soc.* **2014**, *136*, 3553.

(56) Dudev, T.; Lim, C. *Sci. Rep.* **2015**, *5*, 7864.

(57) Dudev, T.; Musset, B.; Morgan, D.; Cherny, V. V.; Smith, S. M. E.; Mazmanian, K.; DeCoursey, T. E.; Lim, C. *Sci. Rep.* **2015**, *5*, 10320.

(58) *Gaussian I*; Pittsburgh, PA, 2000−2003.

(59) Frisch, M. J.; Trucks, G. W.; Schlegel, H. B.; Scuseria, G. E.; Robb, M. A.; Cheeseman, J. R.; Scalmani, G.; Barone, V.; Mennucci, B.; Petersson, G. A.; Nakatsuji, H.; Caricato, M.; Li, X.; Hratchian, H. P.; Izmaylov, A. F.; Bloino, J.; Zheng, G.; Sonnenberg, J. L.; Hada, M.; Ehara, M.; Toyota, K.; Fukuda, R.; Hasegawa, J.; Ishida, M.; Nakajima, T.; Honda, Y.; Kitao, O.; Nakai, H.; Vreven, T.; Montgomery, J. A., Jr.; Peralta, J. E.; Ogliaro, F.; Bearpark, M.; Heyd, J. J.; Brothers, E.; Kudin, K. N.; Staroverov, V. N.; Kobayashi, R.; Normand, J.; Raghavachari, K.; Rendell, A.; Burant, J. C.; Iyengar, S. S.; Tomasi, J.; Cossi, M.; Rega, N.; Millam, J. M.; Klene, M.; Knox, J. E.; Cross, J. B.; Bakken, V.; Adamo, C.; Jaramillo, J.; Gomperts, R.; Stratmann, R. E.; Yazyev, O.; Austin, A. J.; Cammi, R.; Pomelli, C.; Ochterski, J. W.; Martin, R. L.; Morokuma, K.; Zakrzewski, V. G.; Voth, G. A.; Salvador, P.; Dannenberg, J. J.; Dapprich, S.; Daniels, A. D.; Farkas, O.; Foresman, J. B.; Ortiz, J. V.; Cioslowski, J.; Fox, D. J. *Gaussian 09*; Gaussian, Inc.: Wallingford, CT, 2009.

(60) Wong, M. W. *Chem. Phys. Lett.* **1996**, *256*, 391.

(61) Dudev, T.; Lim, C. *J. Phys. Chem. B* **2012**, *116*, 10703.

(62) Dudev, T.; Mazmanian, K.; Lim, C. *Phys. Chem. Chem. Phys.* **2016**, *18*, 16986.

(63) Gilson, M. K.; Sharp, K. A.; Honig, B. H. *J. Comput. Chem.* **1988**, *9*, 327.

(64) Lim, C.; Bashford, D.; Karplus, M. *J. Phys. Chem.* **1991**, *95*, 5610.

(65) Bashford, D. In *Scientific Computing in Object-Oriented Parallel Environments*; Ishikawa, Y., Oldehoeft, R., Reynders, J. W., Tholburn, M., Eds.; Springer: Berlin Heidelberg, 1997; Vol. *1343*, p 233.

(66) Dudev, T.; Lim, C. *J. Am. Chem. Soc.* **2006**, *128*, 1553.

DOI: 10.1021/jacs.6b08041
J. Am. Chem. Soc. 2016, 138, 13038−13047

(67) Reed, A.; Weinstock, R.; Weinhold, F. *J. Chem. Phys.* **1985**, *83*, 735.
(68) Brooks, B. R.; Bruccoleri, R. E.; Olafson, B. D.; States, D. J.; Swaminathan, S.; Karplus, M. *J. Comput. Chem.* **1983**, *4*, 187.
(69) Pearson, R. G. *J. Am. Chem. Soc.* **1986**, *108*, 6109.
(70) Smith, R. M.; Martell, A. E. *Critical Stability Constants*; Plenum Press: New York, 1989; Vol. *2*, Suppl. 2.
(71) Kelly, C. P.; Cramer, C. J.; Truhlar, D. G. *J. Chem. Theory Comput.* **2005**, *1*, 1133.
(72) Friedman, H. L.; Krishnan, C. V. In *Water: A Comprehensive Treatise*; Franks, F., Ed.; Plenum Press: New York, 1973; Vol. *3*, p 1.
(73) Ben-Naim, A.; Marcus, Y. *J. Chem. Phys.* **1984**, *81*, 2016.
(74) Wolfenden, R. *Biochemistry* **1978**, *17*, 201.
(75) Chambers, C. C.; Hawkins, G. D.; Cramer, C. J.; Truhlar, D. G. *J. Phys. Chem.* **1996**, *100*, 16385.
(76) Wolfenden, R.; Andersson, L.; Cullis, P. M.; Southgate, C. C. B. *Biochemistry* **1981**, *20*, 849.
(77) Eigen, M. *Angew. Chem., Int. Ed. Engl.* **1964**, *3*, 1.
(78) Huggins, M. L. *J. Phys. Chem.* **1936**, *40*, 723.
(79) Zundel, G. *Angew. Chem., Int. Ed. Engl.* **1969**, *8*, 499.
(80) Dudev, T.; Lim, C. *Phys. Chem. Chem. Phys.* **2012**, *14*, 12451.
(81) Thomaston, J. L.; Alfonso-Prieto, M.; Woldeyes, R. A.; Fraser, J. S.; Klein, M. L.; Fiorin, G.; DeGrado, W. F. *Proc. Natl. Acad. Sci. U. S. A.* **2015**, *112*, 14260.
(82) DeCoursey, T. E. *Physiol. Rev.* **2003**, *83*, 475.
(83) Begenisich, T.; Danko, M. *J. Gen. Physiol.* **1983**, *82*, 599.
(84) Mozhayeva, G. N.; Naumov, A. P.; Negulyaev, Y. A. *Gen. Physiol. Biophys.* **1982**, *1*, 5.
(85) Mozhayeva, G. N.; Naumov, A. P. *Pfluegers Arch.* **1983**, *396*, 163.

DOI: 10.1021/jacs.6b08041
J. Am. Chem. Soc. 2016, 138, 13038−13047